Machine learning assisted early anomaly detection of LEDs with spectral power distribution modeling

Liu, Minne; Ibrahim, Mesfin S.; Wen, Minzhen ; Li, Sheng; Wang, An ; Zhang, Guoqi; Fan, Jiajie

DOI
10.1109/SSLChinaIFWS57942.2023.10071010

Publication date
2023

Document Version
Final published version

Published in
Proceedings - 2022 19th China International Forum on Solid State Lighting and 2022 8th International Forum on Wide Bandgap Semiconductors, SSLCHINA

Machine learning assisted early anomaly detection of LEDs with spectral power distribution modeling

Minne Liu[1], Mesfin S. Ibrahim[3], Minzhen Wen[1], Sheng Li[6], An Wang[6], Guoqi Zhang[4] and Jiajie Fan[1,2,4,5*]
[1] Institute of Future Lighting, Academy for Engineering & Technology, Fudan University, Shanghai 200433, China
[2] State Key Laboratory of Applied Optics, Changchun Institute of Optics, Fine Mechanics and Physics, Chinese Academy of Sciences, Changchun 130033, China
[3] Centre for Advances in Reliability and Safety, New Territories, Hong Kong
[4] EEMCS Faculty, Delft University of Technology, 2628 Delft, The Netherlands
[5] Fudan Zhangjiang Institute, Shanghai 201203, China
[6] Shanhai Yaming Lighting Co.Ltd, Shanghai 310000 , China
*Corresponding author: Jiajie Fan, jiajie_fan@fudan.edu.cn

2022 19th China International Forum on Solid State Lighting & 2022 8th International Forum on Wide Bandgap Semiconductors (SSLCHINA: IFWS) | 979-8-3503-4638-1/23/$31.00 ©2023 IEEE | DOI: 10.1109/SSLChinaIFWS57942.2023.10071010

Abstract

Spectral power distribution (SPD) is the radiation power intensity at different wavelengths, containing the most basic photometric and colorimetric performance of the illuminant, which is able to predict the lifetime of LEDs. This paper proposes an SPD model assisted by machine learning algorithms to detect the early failure of white LEDs. The SPD features of 3W high-power white LEDs were firstly extracted by the statistical models of Gaussian, Lorentz, and Asym2sig functions. An unsupervised learning method, principal component analysis (PCA), was then used to reduce the extracted features parameters' dimensions. Next a K-nearest neighbor (KNN)-based method was used to detect LEDs' anomalies by dividing the main cluster into groups, and estimating the distance from the center of mass of each cluster to the test point. The results showed the following: (1) for selected white LEDs, the Asym2sig function has a better fitting result than Gaussian and Lorentz functions; (2) machine learning methods can significantly assist in LED anomaly detection and can decrease the amount of anomaly detection time to 789.6 h, compared to the 1311 h when lumen maintenance degradation reaches 70% as required by IES TM-21.

Keywords: White LEDs; Spectral power distribution; Anomaly detection; Principal component analysis; K-nearest neighbor

1. Introduction

Light-emitting diodes (LEDs), as advanced solid-state lighting, can directly convert electrical energy to light energy without other energy conversions and have been used in fields such as indoor-outdoor lighting [1], automotive and locomotive headlighting, architectural and road lighting, and vegetation lighting [2]. Long service life, high luminous efficiency, high reliability, environmental friendliness, and compact size are LEDs' great strengths [3, 4], which are superior to traditional illuminants.

Many studies related to the fault diagnosis and lifetime prediction of LEDs have been conducted. IES TM-21/28 use luminous flux and chromaticity shift as standard performance indicator for LED light source or lamp's lifetime prediction. In the standard performance, the length of time, when the luminous flux output of a lighting product decreases to 70% of its initial value, is determined as LEDs' service lifetime [5]. According to IES-LM-80, released by the Illuminating Engineering Society of North America (IESNA) in 2008, colorimetric data are required to be collected every 1000 h for a duration of at least 6000 h [6]. Fan *et al*. [7] proposed a method to detect anomalies in white LEDs by calculating the martingale distance between indirect LED performance data (e.g., lead temperature, input drive current, and forward voltage). Cao *et al*. [8] recommended a method to predict LED array modules' luminous flux, using ANN and verified its accuracy by comparing various operating conditions. Jing *et al*. [9] used a constant-drift Wiener process to model the radiation power degradation of the UV LEDs.

Although previous studies on LED lifetime prediction and fault diagnostics have focused on lumen degradation, color shifts have been given insufficient attention. Color degradation is an important performance parameter for LEDs in application scenarios such as museums, supermarkets, and shopping centers. Based on the spectral power distribution (SPD), the most basic luminescence mechanism of illuminant is included by the radiation power distribution emitted by illuminant in a certain visible wavelength range. LEDs' luminosity and chromaticity parameters, such as color coordinates, luminous flux, color rendering index, associated color temperature, can be calculated based on the SPD function.

Thus, the SPD-based design and research can fully consider both lumen degradation and color shift degradation modes. To realize the early fault detection of both lumen degradation and color shift of a white LED, this paper proposes a fault diagnosis method by analyzing the SPD, using principal component analysis and KNN dimension-reduction methods. Accordingly, the present study demonstrates a method to predict the remaining useful lifetime of phosphor-converted white LEDs (pc-WLEDs) through the photometric and colorimetric parameters of the device. Chang *et al*. [10]extracted the same number of points from each lamp and used the training and test data together to obtain a new threshold. In his study, die's and phosphor's SPDs were disassembled, and the anomalies in die, phosphor and entier SPD were diagnosed separately. Results show that degradation of die degradation is earlier than that of phosphor degradation. Using 640 data points, anomalies were first detected from die and then from phosphor, within approximately 1200 hours die's SPD data.

2. Experimental setup and SPD data collection

As shown in Figure 1, the Avago 3W high-power pc-WLEDs (ASMT-JN31-NTV01) were used in this study [11]. The 16 test samples driven by 200 mA DC current were aged under a constant aging temperature (T_a = 90°C). SPD data were

measured using a spectrometer, where a total of 71 cycles (1633 h) of SPD data were collected. When the lumen maintenance was reduced to about 70%, the ageing test was stopped.

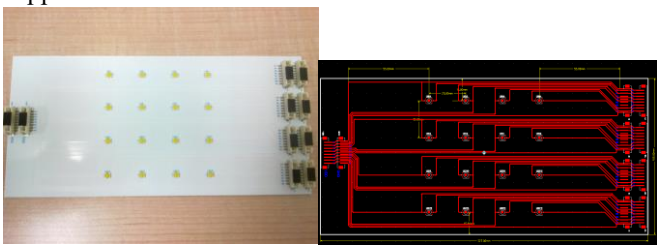

Fig 1. The 3W high-power pc-WLEDs and test board used in this study

3. SPD modeling and features extraction

Most white LEDs on the market use chips covered with phosphor to emit light. Chips emit shortwave light to excite the phosphor, to produce longwave visible light. The remaining light of the chips and the phosphor's emitted light are compounded to form white light. The pc-WLEDs adopts the luminescence mode of blue chips and yellow phosphor, and can indirectly control the intensity ratio of blue and yellow light by regulating the concentration of phosphor, to obtain white light with different color temperatures.

The spectrum of a pc-WLED usually has multiple peaks: one peak is located in the short-wave region (380–495 nm), representing the blue light emitted by the LED chip, i.e., emission spectrum; conversion spectrum is located in the long-wave region (495–745 nm), representing the yellow-green light converted by the phosphor (Figure 2).

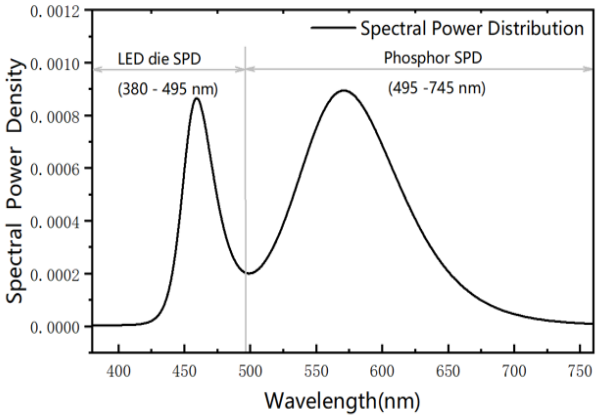

Fig 2. Illustration of SPD of a typical of pc-WLED

Failure modes of pc-WLEDs mainly are highly related to LED chip failure, phosphor failure, and packaging material failure [12]. After a long operating time, the deviation of SPD can be used to determine the failure modes: 1) when LED chips degrades the two spectral areas decline in equal proportion because the intensity of the phosphor-conversion light depends on the intensity of the emitted blue light; 2) when phosphors degrades, the degradation of the conversion spectral area is larger than that of the emission spectral area; 3) when packaging materials fail, the degradation of the emission spectral area is larger because the packaging materials, typically silicone, are more sensitive to short wavelength light.

Thus, the SPD of a pc-WLED always can be modeled by some overlapped single-peak spectra, as follows:

$$SPD_{LED}(\lambda) = \sum_{i=1}^{n} SPD_i(\lambda) \quad (1)$$

where SPD_{LED} represents the spectrum of the LED, SPD_i represents the decomposed SPD spectrum i, and n is the total number of SPDs, which is highly depended on the phosphor materials as used and light conversion mechanisms. Gaussian [13-15], Lorentz, and asymmetric double sigmoidal (Asym2sig) functions are the candidate models to describe the decomposed SPD. Considering a white LED as a double-peaked function, where n equals 2, i.e., functions 1 and 2 are superposed, the models are as follows:

1) Double Gaussian function:

$$y = y_0 + \left(\frac{A_1}{\left(\omega_1\sqrt{\frac{\pi}{2}}\right)} e^{-2\left(\frac{(x-xc_1)}{\omega_1}\right)^2}\right) + \left(\frac{A_2}{\left(\omega_2\sqrt{\frac{\pi}{2}}\right)} e^{-2\left(\frac{(x-xc_2)}{\omega_2}\right)^2}\right) \quad (2)$$

where x is the wavelength, xc_1 and xc_2 are peak wavelengths, and ω_1 and ω_2 represent full widths at half-maxima (FWHM);

2) Double Lorentz Function:

$$y = y_0 + \frac{2A_1}{\pi}\left(\frac{\omega_1}{(4(x-xc_1)^2 + {\omega_1}^2)}\right) + \frac{2A_2}{\pi}\left(\frac{2}{(4(x-xc_2)^2 + {\omega_2}^2)}\right) \quad (3)$$

where A_1 and A_2 represent the areas of the spectra;

3) Double Asym2sig function:

$$y = y_0 + A_1\left(\frac{1}{1+e^{\frac{-\left(x-xc_1+\frac{\omega_{11}}{2}\right)}{\omega_{21}}}}\right)\left(1-\frac{1}{(1+e^{\frac{-\left(x-xc_1-\frac{\omega_{11}}{2}\right)}{\omega_{31}}})}\right) + A_2\left(\frac{1}{1+e^{\frac{-\left(x-xc_2+\frac{\omega_{12}}{2}\right)}{\omega_{22}}}}\right)\left(1-\frac{1}{(1+e^{\frac{-\left(x-xc_2-\frac{\omega_{12}}{2}\right)}{\omega_{32}}})}\right) \quad (4)$$

where A_1 and A_2 represent the amplitude values, ω_{31} and ω_{32} represent the variances of the low-energy side, and ω_{21} and ω_{22} represent the variances of the high-energy side.

Referring to the equations 2 to 4, the 16 sets of collected data were fitted with Double-Gaussian, Double-Lorentz, and Double-Asym2sig functions, respectively. The fitting curves are shown in Figure 3. The Goodness-of-fitting is judged by the coefficient of determination,

$$R^2 = 1 - \frac{\sum_{i=1}^{n}(\hat{y}_i - y_i)^2}{\sum_{i=1}^{n}(\bar{y}_i - y_i)^2} \quad (5)$$

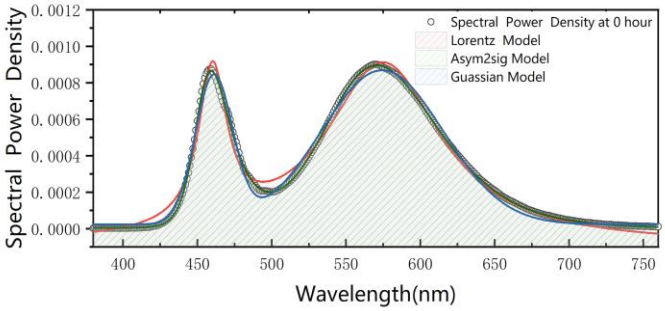

Fig 3. SPD modeling with three function fitting curves

Table 1 The Goodness-of-fitting results of three SPD models

Models	Goodness-of-fitting R^2
Double-Gaussian function	0.991124
Double-Lorentz Function	0.98510267
Double-Asym2sig function	0.99952867

As shown in Table 1, all three curves fitted well with R^2 is at least 95%. Compared with the R^2 of the three curves, the

979-8-3503-4638-1/22/$31.00 ©2022 IEEE

Double-Asym2sig function has the best fitting result, reaching 99.9%. Therefore, the Double-Asym2sig function was used in the further study for SPD modeling and feature extraction.

4. Principal component analysis and K-means method

As the most commonly used linear dimensionality reduction method, Principal component analysis (PCA) maps high-dimensional data to a low-dimensional space by some linear projection, where the data are most informative in the projected dimension. Hence, PCA uses less data dimensions to retain more characteristics of original data points. The failure points were detected by extracting 11 eigenvalues and transforming them into principal components as initial values. To analyze the effect of the training data on experimental results, LEDs 2, 4, 8, and 10 of 16 LEDs were used as test data, where each LED included 72 data points. Each training dataset was used to evaluate PCA's variance-covariance matrix. Original training set was projected onto the selected features vector to obtain a new dimension after dimensionality reduction. In Figure 4, the 11 features extracted by SPD were reduced to two principal components, in which the x-axis indicates the dimension of principal component, and the y-axis indicates the variance of the corresponding principal component. Gently fluctuating points were removed, and the two principal components were retained.

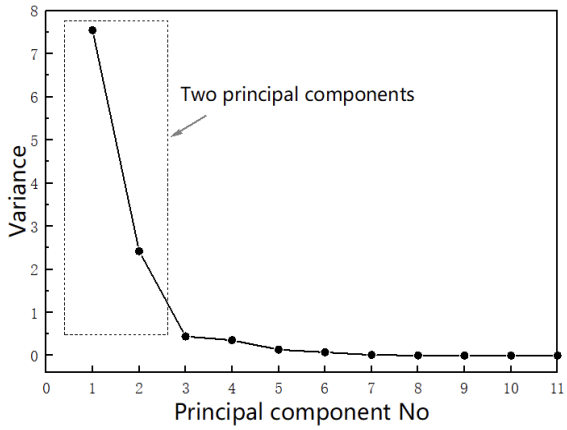

Fig 4. Principal component for SPD training data using 720 data points (72 points from each LED)

KNN-means belongs to the class of unsupervised learning in machine learning, which uses unlabeled data to learn the distribution of data and the relationships between data. The "k" in the K-means algorithm represents k clusters, and the "means" indicates, after dividing into new clusters, the center of mass of each cluster is recalculated according to the averaging approach, thus determining the new cluster center. Total cluster sum of squares is obtained by summing the intra-cluster sums of squares of all clusters in the dataset, as follows:

$$CSS = \sum_{j=0}^{m} \sum_{i=1}^{n} (x_i - \mu_i)^2 \quad (6)$$

where observations ($x_1, x_2, x_3 \ldots x_n$) are one-dimensional vectors, and KNN-means clustering divides the n observations into m clusters, S ($S_1, S_2, S_3 \ldots S_m$), where the center of mass of cluster S_i is μ_i. The smaller the total inertia, the more similar the samples within each cluster, and the more effective the clustering. Through continuous iteration, we achieve the best cluster selection when inertia minimizes the centroid.

For a dataset with 720 training points, the training set was divided into four clusters, as shown in Figure 6. In Figure 5, it is observed that the curve becomes smooth at cluster 4. Based on the multiple optical features of the LEDs, the dataset was divided into four groups instead of two or three. The 720 training sets were trained with two and three groups for anomaly detection, but no anomaly was found in any of the results, so the 720 datasets were considered to be divided into four clusters, as shown in Figure 6 where the x-axis and y-axis represent principal components 1 and 2, respectively.

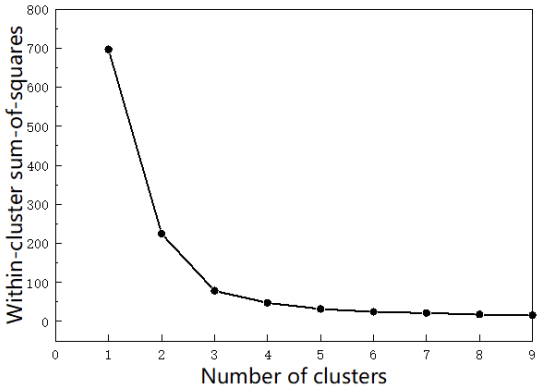

Fig 5. CSS for SPD training data using 720 data points

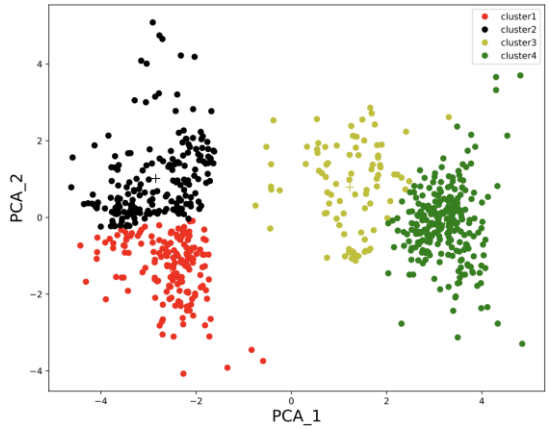

Fig 6. KNN-means for SPD training data using 720 data points

After dividing training set into four clusters by KNN-means, similarity detection can be used to determine the failure point. When dividing training data into m clusters, the center of mass of cluster S_i is μ_i, and the distance from the data point to the center of mass is calculated by the Euclidean distance. The distance (D_i) from each test point to the center of mass (μ_i) to which it belongs is evaluated. When D_i is larger than the threshold (T_i), it is judged to be an anomaly, and when it is smaller, then the step is repeated at the next test point. The average radius (R (S_j)) is the average distance of all points in the cluster to the center of mass μ_j, which measures the density of points in the cluster. The following equations calculate the center of mass and radius[10]:

$$\mu_j = \frac{\sum_{i=1}^{k} \mu_i}{k} \quad (7)$$

$$\mathrm{R}(S_j) = \sqrt{\frac{\sum_{i=1}^{k} (\mu_i - \mu_j)^2}{k}} \quad (8)$$

Ideally, the clusters appear as circles. In Figure 6, each cluster is closer to an ellipse, with different major and minor axes. The failure point diagnosis depends on the accuracy of

979-8-3503-4638-1/22/$31.00 ©2022 IEEE

the threshold value, and the failure threshold should be between the long and short axis, and too large or small is not conducive to the error point diagnosis. When the threshold is too large, the missed-alarm rate increases, and when it is too small, the failure detection rate increases. To increase the accuracy while considering the distribution of detection points, the new threshold is therefore adjusted as:

$$Detection\ threshold(\mathrm{T}) = \text{mean radius(r)} + \frac{standard\ deviation(\sigma)}{dimensional\ factor(d)} \quad (8)$$

where σ is the standard variance, describing the offset of the test point from the center. D is the scaling factor, which in this study is 2, because the data are two-dimensional after dimensionality-reduction.

4. Anomaly detection results and discussion

In this section, ten of these datasets, a total of 720 data points, were used as the training set to examine LED 16. When the training set was two clusters and three clusters, no alarm was detected, as shown in Figures 7 and 8. When the training cluster was four clusters, the failure point was found and the anomaly was monitored. When the distance from the center of mass Dj was greater than the threshold Tj, an alarm was detected to detect failure at 789.6 h, an anomaly occurred as shown in Figure 9.

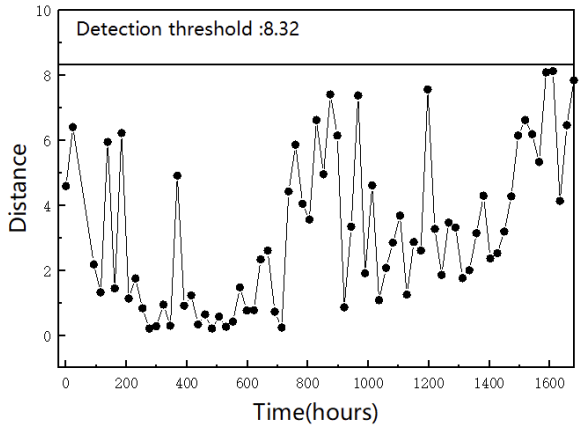

Fig 7. Distance measure of cluster 2 from LED 16

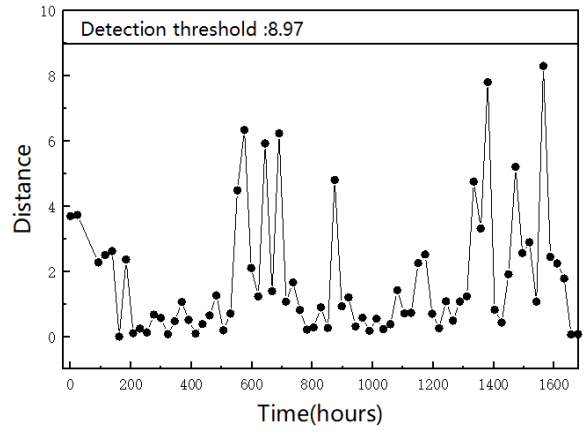

Fig 8. Distance measure of cluster 3 from LED 16

Next, the training data were placed into 2, 4, 6, 8, 10 and 12 groups, that is144, 288, 432, 576, 720 and 864 data points, respectively, to verify the anomaly detection accuracy of the remaining 14, 12, 10, 8, 6 and 4 LEDs separately. The error detection was roughly divided into two groups: false alarm and missed alarm. A false alarm refers to the premature detection of an anomaly, i.e., the LED is judged to fail while in normal condition; a missed alarm means that no anomaly is detected when the LED ends its life (luminous flux degrades to 70% or color shift reaches 0.007).

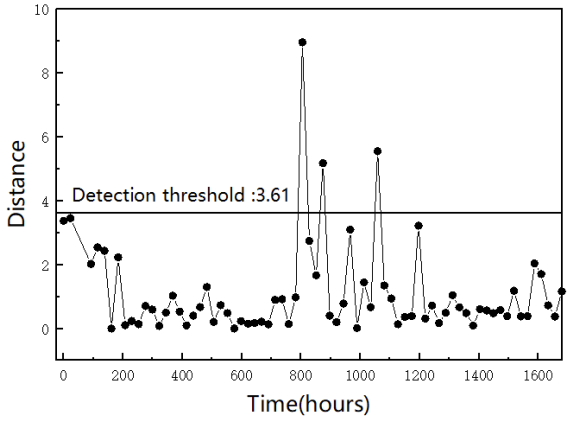

Fig 9. Distance measure of cluster 4 from LED 16

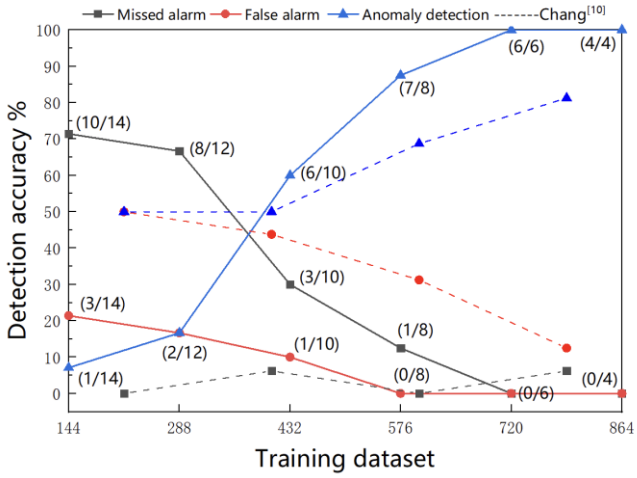

Fig 10. Anomaly detection results (Missed alarm rate, False alarm rate, and Anomaly detection rate)

The anomaly detection results are shown in Figure 10, which indicates that both missed alarms and false alarms showed a decreasing trend with the increase of training data. When the data reaches 576 and 720 respectively, the false alarm and missed alarm reach 0, and no such error occurs. Meanwhile, the anomaly detection accuracy shows an increasing trend. Moreover, after the training data reached 720, there were no missed or false alarms. Compared to the work from Chang[10], in this paper, the training data and testing data were separated, and only testing dataset were used to verify the accuracy of the proposed method. Fuethermore, in the dimensionality reduction, there were three parameters after dimensionality reduction in [10], but only two dimensions in this paper and the clusters were relatively less. The reduction of dimensionality as well as the number of clusters makes the subsequent steps much simpler. When the dataset reaches 397, the anomaly detection accuracy is higher than that from [10]. Meanwhile, the false alarm rate is lower, and the accuracy of missed alarm is comparatively higher. This may be caused by a higher threshold as compared to Chang's, which leads to more points

979-8-3503-4638-1/22/$31.00 ©2022 IEEE

gathered in the same cluster, and a larger radius and a larger threshold were finally obtained.

5. Conclusion

In this paper, we proposed a machine learning-assisted anomaly detection method, which first used the superposition of two asymmetric Asym2sig functions to fit the SPD of pc-WLEDs, where the functions could describe the spectra of blue light chips and yellow light phosphor conversions best. The extracted features take full advantage of the information contained in the SPD, not just the lumen degradation, but also the color shift. Eleven extracted features were reduced to two by PCA and KNN-means was used for clustering after dimension reduction. A new threshold was obtained by the above distance formula after grouping. When the distance from the test data to the center of mass exceeded the threshold, an anomaly was detected. The results show that: according to the IES TM-21, when the lumen degradation was 70%, the time required for this accelerated experiment was 1311 h, which was reduced to 789.6 h by the proposed method, thereby significantly reducing the time required for LED reliability tests.

Acknowledgements

The work described in this paper was partially supported by the National Natural Science Foundation of China (51805147), State Key Laboratory of Applied Optics (SKLAO2022001A01), Shanghai Science and Technology Development Foundation (21DZ2205200) and Shanghai Pujiang Program (2021PJD002).

References

[1] S. Liu and X. Luo, "LED Packaging for Lighting Applications: Design, Manufacturing, and Testing," 2011.

[2] M. R. Sabzalian *et al.*, "High performance of vegetables, flowers, and medicinal plants in a red-blue LED incubator for indoor plant production," *Agronomy for Sustainable Development,* vol. 34, no. 4, pp. 879-886, 2014/10/01 2014, doi: 10.1007/s13593-014-0209-6.

[3] M. H. Chang, D. Das, P. V. Varde, and M. Pecht, "Light emitting diodes reliability review," *Microelectronics and reliability,* 2012.

[4] W. V. Driel, "Solid State Lighting Reliability Components to Systems."

[5] *Projecting Long Term Lumen Maintenance of LED Light Sources*, 2015.

[6] L. Refrigerated and D. C. Lighting, "Measurements of Solid-State Lighting Products" 2. IES LM-80-08, "Approved Method for Measuring Lumen Maintenance of LED," 2010.

[7] J. Fan, C. Qian, X. Fan, G. Zhang, and M. Pecht, "In-situ monitoring and anomaly detection for LED packages using a Mahalanobis distance approach," in *2015 First International Conference on Reliability Systems Engineering (ICRSE)*, 2015: IEEE, pp. 1-6.

[8] Y. Cao, W. Yuan, W. Chen, M. Li, J. Fan, and G. Zhang, "Predicting of luminous flux for a LED array using artificial neural network," in *2020 21st International Conference on Thermal, Mechanical and Multi-Physics Simulation and Experiments in Microelectronics and Microsystems (EuroSimE)*, 2020: IEEE, pp. 1-4.

[9] Z. Jing, M. S. Ibrahim, J. Fan, X. Fan, and G. Zhang, "Lifetime prediction of ultraviolet light-emitting diodes with accelerated Wiener degradation process," in *2019 20th International Conference on Thermal, Mechanical and Multi-Physics Simulation and Experiments in Microelectronics and Microsystems (EuroSimE)*, 2019: IEEE, pp. 1-8.

[10] M.-H. Chang, C. Chen, D. Das, and M. Pecht, "Anomaly detection of light-emitting diodes using the similarity-based metric test," *IEEE Transactions on industrial informatics,* vol. 10, no. 3, pp. 1852-1863, 2014.

[11] D. S. ASMT-Jx3x, "3W Mini Power LED Light Source," *Avago Technologies: San Jose, CA, USA,* 2012.

[12] J. Fan, M. G. Mohamed, C. Qian, X. Fan, G. Zhang, and M. Pecht, "Color shift failure prediction for phosphor-converted white LEDs by modeling features of spectral power distribution with a nonlinear filter approach," *Materials,* vol. 10, no. 7, p. 819, 2017.

[13] R. Lu, Q. Hong, Z. Ge, and S.-T. Wu, "Color shift reduction of a multi-domain IPS-LCD using RGB-LED backlight," *Optics Express,* vol. 14, no. 13, pp. 6243-6252, 2006.

[14] B.-M. Song and B. Han, "Spectral power distribution deconvolution scheme for phosphor-converted white light-emitting diode using multiple Gaussian functions," *Applied optics,* vol. 52, no. 5, pp. 1016-1024, 2013.

[15] C. Qian, J. Fan, X. Fan, and G. Zhang, "Prediction of lumen depreciation and color shift for phosphor-converted white light-emitting diodes based on a spectral power distribution analysis method," *IEEE Access,* vol. 5, pp. 24054-24061, 2017.

979-8-3503-4638-1/22/$31.00 ©2022 IEEE